Mobility-based Path Planning and Evaluation Strategy for Exploration Rover

Genya Ishigami

Institute of Space and Astronautical Science, Japan Aerospace Exploration Agency

Abstract : In this paper, a path planning and evaluation method that explicitly considers dynamic mobility of the rover is presented. The proposed method consists of the following three steps. First, various paths on a given terrain map are generated with varying weighting factors for path planning algorithm. Each path is then examined through dynamic simulations of the rover in which the rover travels along with the path. The simulation result provides a metric for robotic mobility such as stability of the rover and wheel slippage. The simulation also calculates elapsed time and energy consumption required to complete the path traveling. All of the paths are quantitatively evaluated based on the metrics, and then, the most feasible path between them is obtained. Demonstrations for the path planning and evaluation are presented in this paper that confirms the usefullness of the proposed method.

探査ローバの走行特性に基づいた経路計画と経路評価手法の提案

石上 玄也

宇宙航空研究開発機構 宇宙科学研究所

摘要 : 本論文では，不整地上を走行する探査ローバがより安全な走行経路を生成する手法を提案する．本手法は，ローバの動的な走行特性を考慮した評価を経路生成のスキームに取り込むことによって，最適な経路を選択するアプローチであり，具体的には以下の 3 つのステップより構成される．(1）経路計画アルゴリズムにおける重み関数を変化させ，候補となる経路をいくつか生成し，(2）各経路について，動力学を考慮したローバの走行シミュレーションを行い，(3）シミュレーションから得られるローバの動的な走行特性から最適な経路を選択する．本論文では，提案手法の詳細ならびに数値シミュレーションによる実証結果について述べる．

1. Introduction

Mobile robots on planetary surface exploration have been performing a significant role to accelerate valuable scientific missions. On challenging terrain of the planetary surface, the rover should evade mobility hazards such as immobilizing wheel slip on loose sand, collision with obstacles, or rollover on sloped terrain. Therefore, the rovers are required to travel over a rough terrain, with navigating itself by observing the terrain around the rover and planning a feasible path to be traveled.

There have been substantial works dealing with path/motion planning algorithms for mobile robots, such as the A* and D* methods[1], the potential field approach[2], the probabilistic roadmap technique[3], and the rapidly-exploring random tree (RRT) algorithm[4]. Randomized approaches to kinodynamic motion planning reported in[5] is an efficient tool for the purpose of path generation, with RRTs proving to be a highly effective framework. Also, heuristically-biased expansion for generation of efficient paths with satisfying dynamic constraints has been developed by[6]. Explicit modeling of a robot's closed-loop controller in the planning method, which results in trackable paths, has been studied in[7]. Path generation techniques that consider robotic mobility have also been investigated. For example, a trajectory generation method on rough terrain with taking into account predictable vehicle dynamics has been proposed by [8]. A planning algorithm with model based evaluations, that include uncertainties of the terrain measurement and rover localization, has been developed in[9]. In addition, a terrain traversability index with fuzzy logic for mobile robot navigation has been introduced in[10], and a map along with the terrain traversability has been used for path planning of planetary rovers[11].

The methods noted above have been applied several types of mobile robot and their usefulness have been validated. However, assessments for dynamic mobility of the robots in the path planning process have not been explicitly addressed. In particular, the planetary rover must carefully generate a feasible path in accordance with its mobility performance. This is because of the constraints on planetary exploration, such as limited capacity/bandwidth for the information of environment, time delay between the rover and the Earth, and limited electric power available.

The robotic mobility for planetary rover has been investigated in several works. A multibody system for deterministic simulation of rover tire-soil interaction has been demonstrated[12]. A terramechanics-based dynamic model for the rover that considers wheel slips and traction forces has been developed in the authors' previous work[13]. The mobility

prediction of the rover in uncertain terrain has been investigated[14]. Some recent work has attempted to predict rover mobility on slopes via learning-based approach[15].

Exploiting the background for the mobility analysis, this paper presents a path planning and evaluation strategy that explicitly considers the dynamic mobility of rover. The proposed strategy consists of the following three-step approach.

First, a path planning algorithm generates various possible paths on a given terrain map. The paths generated vary according to weightings for individual costs (terrain roughness, terrain inclination, and path length) in the path planning algorithm. Typical "candidate paths" are extracted from all of the different least-cost paths by eliminating similar paths among them.

Subsequently, each candidate path is examined through dynamic simulation. A key technique in the simulation is a wheeled vehicle model comprised of two sub-models: a vehicle dynamic model of the rover to obtain mobility profiles, and a wheel-terrain contact model to calculate the wheel interaction forces on deformable soil at each dynamic simulation step. The dynamic simulation also checks whether the rover can track the candidate path or not.

As the last step, every candidate path is quantitatively evaluated based on a metric provided by the dynamic simulation. The metric, termed a dynamic mobility index, is composed of stability of the rover (roll and pitch), wheel slippage, and elapsed time and total energy required to complete the path travel. In this work, the most feasible path is found as a path which requires the least energy consumption since the energy consumption is assumed as a gross cost of the rover stability, the wheel slippage, and the elapsed time; less mobility of the rover generally needs more energy to traverse rough terrain, and also, the total energy consumption is in proportion to the elapsed time.

This paper is organized as follows: Section 2 describes the path planning algorithm for the generation of various candidate paths. Section 3 introduces the wheeled vehicle model for the dynamic simulation. The dynamic mobility index used for the path evaluation is presented in Section 4. Demonstrations for the proposed strategy are addressed in Section 5.

2. Path Planning Algorithm

For the path planning in this work, it is assumed that three dimensional terrain information around rover is given without any uncertainties. As illustrated in Fig. 1, the terrain map is represented as the digital elevation map (DEM) defined by a series of elevations along with discretized nodes. The DEM can be created from a point cloud data of 3D terrain feature measured by a stereo camera pair or a laser range finder that may be mounted on the rover.

The i-th node n_i, defined as "current node", locates the position of the rover in the map and it varies from 1 to N^2. One single node connects with eight adjacent surrounding nodes, allowing the rover to head for eight possible directions from its current node.

Robotic mobility in the path planning is important in field conditions in which terrain inclination, roughness, and mechanical properties can significantly impede rover's mobility. The path planning algorithm in this work considers three indices: terrain roughness, terrain inclination, and path length. A criteria function composed of these indices along with varied weighting factors generates various paths.

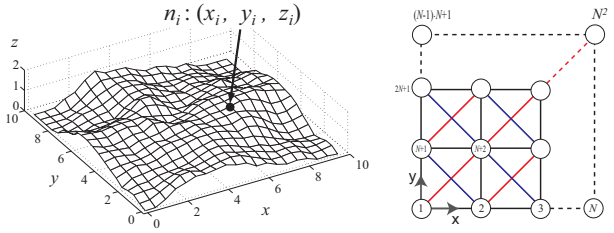

Fig. 1 : Terrain map represented by DEM. Right figure shows the node connectivity between the adjacent nodes. N is the number of nodes per length of the terrain map.

2.1 Terrain Roughness Index

The terrain roughness is related to traversability of a rover. In order to exclude uneven bumpy areas from a path to be traveled, the terrain roughness index B_{ij} is defined as a standard deviation of the terrain elevation over a projection region of a rover R_{ij}:

$$B_{ij} = \sqrt{\frac{1}{n}\sum_{R_{ij}} \big(z(R_{ij}) - \bar{z}(R_{ij})\big)^2} \qquad (1)$$

R_{ij} is determined by a dimension of the rover and its longitudinal direction is aligned along with the vector $\vec{n}_{ij}$ composed of the current node n_i and adjacent node n_j (Fig. 2). Therefore, one current node has eight possible projection regions in accordance with the rover heading. In the above equation, n represents a number of nodes inside the region and $\bar{z}$ denotes an average elevation in R_{ij}. The rougher the terrain around a node, the larger the index at the node becomes.

2.2 Terrain Inclination Index

A rover experiences relatively high wheel slippage when it climbs up or traverses on a sloped terrain. This is because the traction load due to the gravity becomes significant on the sloped terrain. Also, rollover of the rover traversing on a steep slope is another mobility hazard.

The terrain inclination index indicates these risks as well as traversability on sloped terrain. The terrain inclination index is divided into two axes, roll and pitch of the rover (Fig. 3). Each of them is geometrically calculated as the angle between the inertial coordinate and a pseudo-plane composed of wheel contact points at a projection region R_{ij}:

$$\begin{aligned} \text{Roll} &: \Theta_{x_{ij}} = \theta_x(R_{ij}) \\ \text{Pitch} &: \Theta_{y_{ij}} = \theta_y(R_{ij}) \end{aligned} \qquad (2)$$

Note that multiple terrain inclination angles will be given owing to the kinematic configuration of the rover (i.e. a 4-wheeled rover may have four contact points, resulting in a

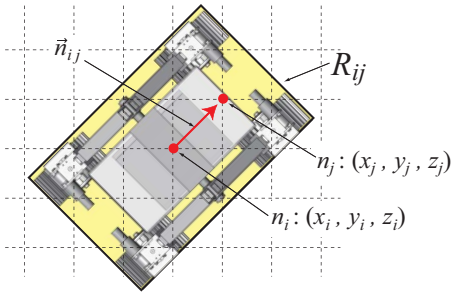

Fig. 2 : Projection region (yellow-colored area) of the rover on terrain map.

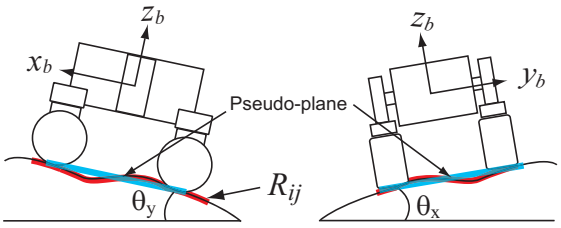

Fig. 3 : Terrain inclination angles. The red curvature depicts the projection region R_{ij} and the blue line depicts the pseudo-plane composed of wheel contact points.

skewed plane at R_{ij}). In such case, the largest inclination angle among them is selected for the index.

2.3 Path Length Index

The path length index performs to find the shortest path from a start to a goal. The path length index L_{ij} is simply calculated as the distance from the current node n_i to adjacent nodes n_j:

$$L_{ij} = |\vec{n}_{ij}| = \sqrt{(x_i - x_j)^2 + (y_i - y_j)^2 + (z_i - z_j)^2} \tag{3}$$

2.4 Criteria Function for Path Planning

A criteria function for the path planning is comprised of the indices introduced in the above subsections:

$$C(\boldsymbol{p}) = \sum_{n_i \in \boldsymbol{p}} \left(W_B \frac{B_{ij}}{N_B} + W_{\theta_x} \frac{\Theta_{xij}}{N_{\theta_x}} + W_{\theta_y} \frac{\Theta_{yij}}{N_{\theta_y}} + W_L \frac{L_{ij}}{N_L} \right) \tag{4}$$

where W_B, W_L, W_{θ_x}, and W_{θ_y} are the weighting factors which assign specific priorities to the corresponding indices. The weighting factors for the terrain inclination indices take a value of infinity if the indices exceed predetermined threshold angles. The threshold angles are given based on the slope traversability of the rover (i.e. maximum slope climbing angle). N_B, N_L, N_{θ_x}, and N_{θ_y} are the normalization factors, each of which takes the maximum value of the corresponding index calculated from the terrain map. The path $\boldsymbol{p}$ consists of a series of neighboring/chained nodes:

$$\boldsymbol{p} = \{n_{start}, \ \cdots, \ n_i, \ n_j, \ \cdots, \ n_{goal}\} \tag{5}$$

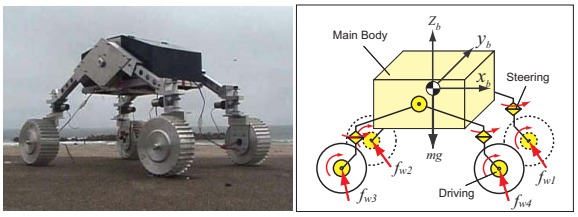

(Rover test bed) (Vehicle dynamic model)

Fig. 4 : Vehicle dynamic model as an articulated multibody system.

For the criteria function in Eq. (4), the smaller each value of the index, the less the mobility hazard on a path becomes. Therefore, the path planning problem is assumed as "shortest path search problem". The conventional Dijkstra's algorithm is used in this work to derive the least-cost path, which provides a minimum value for the criteria function.

Note that the least-cost path varies in accordance with the values of the weighting factors for the individual indices. In the proposed strategy, all possible paths are generated with varying weightings, and then, typical candidate paths are selected by eliminating similar paths among them.

3. Dynamic Simulation Model

As the second step of the proposed approach in this paper, the dynamic simulation of the rover travelling on each candidate path is performed, calculating the dynamic mobility of the rover observed on each path. The dynamic simulation requires two sub-models: a vehicle dynamic model of the rover, and a wheel-terrain contact model. The dynamic simulation model described in this section has been developed and validated in the authors' previous work[13].

The rover addressed in this paper is assumed to be a 4-wheeled vehicle (Fig. 4) and modeled as an articulated multibody system. The dynamic motion of a vehicle for given driving and steering conditions are numerically obtained by successively solving the following motion equation:

$$\boldsymbol{H} \begin{bmatrix} \dot{\boldsymbol{v}}_0 \\ \dot{\boldsymbol{\omega}}_0 \\ \ddot{\boldsymbol{q}} \end{bmatrix} + \boldsymbol{C} + \boldsymbol{G} = \begin{bmatrix} \boldsymbol{F}_0 \\ \boldsymbol{N}_0 \\ \boldsymbol{\tau} \end{bmatrix} + \boldsymbol{J}^T \begin{bmatrix} \boldsymbol{F}_e \\ \boldsymbol{N}_e \end{bmatrix} \tag{6}$$

where $\boldsymbol{H}$ represents the inertia matrix of each body, $\boldsymbol{C}$ is the velocity depending term, $\boldsymbol{G}$ is the gravity term, $\boldsymbol{v}_0$ is the translational velocity of the vehicle, $\boldsymbol{\omega}_0$ is the angular velocity of the vehicle, $\boldsymbol{q}$ is the angle of each joint (such as wheel rotation and steering angle), $\boldsymbol{F}_0 = [0, \ 0, \ 0]^T$ is the forces at the centroid of the vehicle body, $\boldsymbol{N}_0 = [0, \ 0, \ 0]^T$ is the moments at the centroid of the vehicle body, $\boldsymbol{\tau}$ is the torques acting at each joint (driving/steering torques), $\boldsymbol{J}$ is the Jacobian matrix, and $\boldsymbol{F}_e$ and $\boldsymbol{N}_e$ are the external forces and moments acting at the centroid of the wheel, respectively.

The wheel-terrain contact forces, including the drawbar pull F_x, side force F_y, and vertical force F_z, can be calculated by the following equations[13][17]:

$$F_x = rb \int_{\theta_r}^{\theta_f} \{\tau_x(\theta) \cos\theta - \sigma(\theta) \sin\theta\} \, d\theta \tag{7}$$

$$F_y = \int_{\theta_r}^{\theta_f} \{rb\tau_y(\theta) + R_b\,[r - h(\theta)\cos\theta]\}\,d\theta \quad (8)$$

$$F_z = rb\int_{\theta_r}^{\theta_f} \{\tau_x(\theta)\sin\theta + \sigma(\theta)\cos\theta\}\,d\theta \quad (9)$$

where r is the wheel radius, b is the wheel width, $\sigma(\theta)$ is the normal stress beneath the wheel, $\tau_x(\theta)$ and $\tau_y(\theta)$ are the shear stresses in the longitudinal and lateral direction of the wheel. The contact patch of the wheel is determined by the entry angle θ_f and the exit angle θ_r. R_b is a reaction resistance generated by the bulldozing phenomenon on a side face of the wheel.

4. Dynamic Mobility Index for Path Evaluation

The dynamic mobility index used for the path evaluation includes the following metrics: the rover stability, the wheel slippages, and the elapsed time and the energy consumption required for the path travel.

The rover stability is defined as the maximum orientation angles in roll and pitch observed during therover travel on the given path. The wheel slippages are given as maximum slip ratio and slip angle of wheels during the run. The elapsed time is determined as the duration the rover spends to complete the path from the start to the goal. The total energy consumption is calculated as the energy used for the steering and driving maneuvers while the rover pursues the path.

In this work, the most feasible path between the candidate paths is determined as a path which requires the least energy consumption. This is due to the fact that the energy consumption can be assumed as a gross cost of rover stability, wheel slippage, and elapsed time; higher stability of the rover or less wheel slippage decreases the traction load of the rover, resulting in less energy required for rover travel. Also, the shorter the elapsed time, the smaller the total energy consumption becomes. In addition, the electric power available for planetary rover is basically limited by the battery performance as well as the energy generated through solar array panels. Therefore, the path evaluation using the energy consumption is relatively comprehensive and will be feasible approach to practical exploration scenarios.

5. Demonstration for Path Planning and Evaluation

5.1 Simulation Procedure

The simulation procedure of the demonstration for the path planning and evaluation is summarized as follows.

1. Input the terrain elevation map to the path planning algorithm with assigning start and goal points.
2. Generate all possible paths by Eq. (4) with varying weighting factors.
3. Extract typical candidate paths by eliminating similar paths generated at Step 2.
4. Conduct dynamic simulations for each candidate path:
   (a) Derive appropriate steering and driving maneuvers which enables the rover to follow the path.
   (b) Determine steering and driving torques.
   (c) Calculate the wheel forces.
   (d) Solve Eq. (6) and obtain the rover position, orientation, and velocity.
   (e) Return Step 4-(a) until the rover reaches the goal.
5. Calculate the dynamic mobility index.
6. Evaluate the candidate paths and find the most feasible path between them.

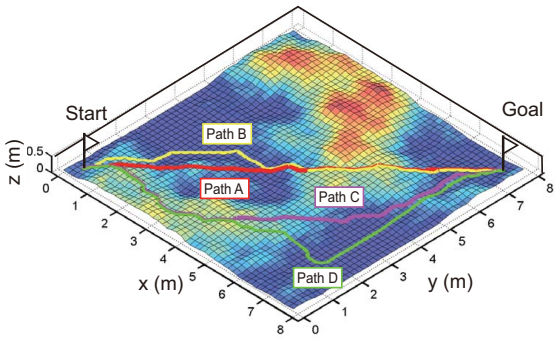

Fig. 5 : Terrain elevation map and typical candidate paths generated.

Table 1. Weighting factors used for the path planning

Path	W_B	W_L	W_{θ_x} W_{θ_y}
Path A	0.25	0.44–0.75	0.000–0.155
Path B	0.25	0.16–0.43	0.160–0.295
Path C	0.25	0.08–0.15	0.300–0.335
Path D	0.25	0.00–0.07	0.340–0.375

5.2 Path Planning

As shown in Fig. 5, the terrain elevation map is given as 8 $\times$ 8 m square with a grid of 50 $\times$ 50 equally-spaced terrain nodes (the total nodes in the map are 2500). The elevation map is obtained by the fractal terrain modeling method[19]. The terrain surface is assumed to be evenly covered with the lunar regolith simulant[20], having constant soil parameters (i.e. cohesion stress, internal friction angle, and others).

As mentioned in Section 2.4, all possible paths were obtained by varying weighting factors. The weighting factor for the terrain roughness index was fixed as 0.25. The weighting factor for the path length was varied from 0.0 to 0.75 with the step of 0.01, while the weighing factors for the terrain inclinations (roll and pitch) were varied such that $W_{\theta_x}(\text{or } W_{\theta_y}) = (0.75 - W_L)/2$, respectively. The thresholds for terrain inclinations were given as 15 degrees. These sets of the uniformly-distributed weighting factors generated 75 paths in total, and then, four typical candidate paths were obtained by eliminating similar paths between them (Fig. 5). The ranges of weighting factors for the four candidate paths are summarized in Table I.

From Fig. 5, it can be seen that Path A is the shortest path directly connecting from the start to the goal, while Path B is similar to Path A but Path B evades a small hill located on

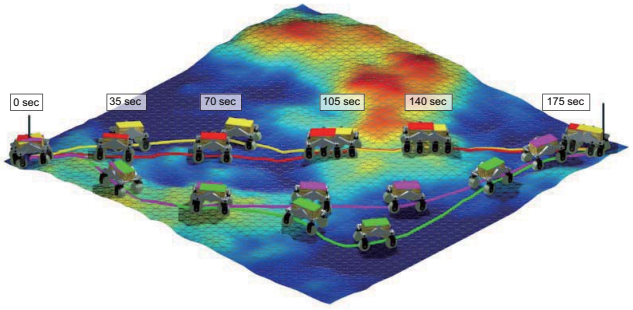

Fig. 6 : Dynamic simulation profile. The red colored rover is for Path A, the yellow is Path B, the purple is Path C, and the green is Path D.

Table 2 : Path Evaluation Result based on Dynamic Mobility Index

Mobility Index	Path A	Path B	Path C	Path D
Roll angle (abs.) (deg)	13.29	7.35	6.02	3.89
Pitch angle (abs.) (deg)	8.35	9.40	5.51	4.64
Slip ratio (-)	0.41	0.41	0.29	0.35
Slip angle (abs.) (deg)	6.80	4.80	7.70	6.70
Elapsed time (sec)	183.1	180.7	193.7	217.5
Energy consumed (Wh)	1.22	1.06	0.98	1.22

Path A. On the other hand, Path C and Path D are generated, bypassing the up-and-down route on Path A or Path B. It is deduced that Path D may be the safest path between the four candidate paths though the length of the path is the longest between them.

5.3 Path Evaluation and Discussion

Four candidate paths were examined through the dynamic simulation. In the simulation, each candidate path is sequentially smoothed by 5th order polynomial approximation with every 7 nodes in the path. The desired traveling velocity was given as 0.06 m/s.

The dynamic motion profile of the rover at each candidate path is shown in Fig. 6. Time histories of the rover's orientations and the electric power used by the driving and steering actuators are shown in Fig. 7 and Fig. 8, respectively. Table II summarizes the dynamic mobility indices on each path.

From the figures and the table, first, it can be clearly seen that the rover orientations on Path A and Path B are less stable as compared to those of Path C and Path D. In particular, the rover traveling on Path A may have a hazard of rollover, which is measured as -13.3 degrees.

The rover on Path B reached the goal with the shortest elapsed time even though the path length of Path B is not the shortest. The rover traveling on Path A, the path length of which is the shortest, experienced relatively large deviation around the roll orientation between 10 to 60 seconds, which induced an increase of the electric power. This is because the terrain roughness/inclinations on Path A required more power and longer seconds for rover travel. On the other hand, the rover on Path D required the longest elapsed time to reach the goal because the path length was the longest,

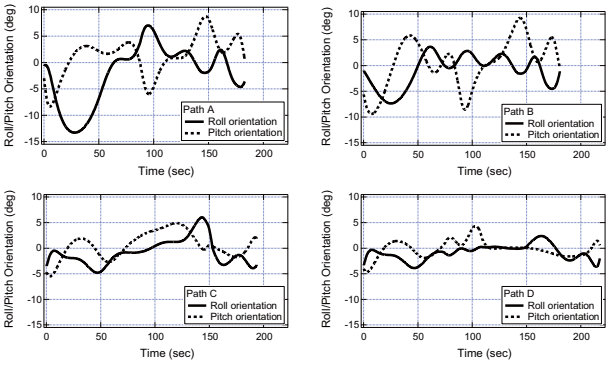

Fig. 7. Time histories of the rover orientations (roll and pitch).

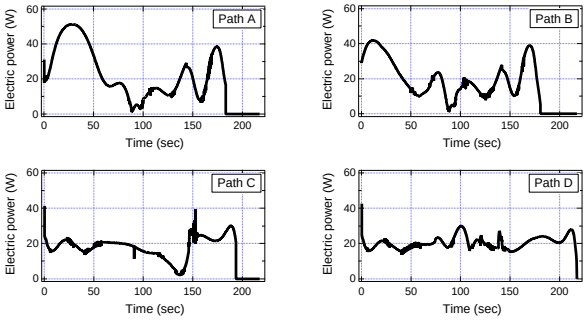

Fig. 8 : Time histories of the electric power used by the rover actuators.

evading all possible mobility hazards on the terrain map.

From Table II, it should be emphasized that the total energy consumed on Path-A is equal to that on Path D. This is due to the fact that the rover on Path A required large energy in order to traverse the sloped terrain. Also, the average electric power on Path D was about 20 W but it was accumulated during the rover travel, resulting in such large energy consumption. The rover on Path B could save the energy by bypassing the hill located on Path A. In addition, it is reasonable that the least energy consumption is observed on Path C since the path was designed as a moderate one between the path length and mobility hazards.

The characteristics of the paths are summarized as follows: Path A is generated as the shortest path length, but it has several potential chances of mobility hazards, consuming large energy for rover travel; Path B is the shortest in the elapsed time, but the maximum pitch angle is the largest (about 10 degrees), requiring the rover to climb such relatively steep slope; Path C enables the rover to travel toward the goal with the lowest wheel slippages, good stability, and the least energy consumption; Path D is the safest path between these four candidate paths, but the rover traveling on this path needs an energy as much as the rover on Path A does.

Based on the evaluation for the candidate paths as discussed above, it is reasonable to conclude that the most feasible path is Path C since the path requires the least energy consumption with less chance of mobility hazards.

6. Conclusion

In this paper, a path planning and evaluation strategy for planetary rovers has been addressed. The proposed strategy is composed of three steps: generation of various candidate paths on a given terrain map, dynamic simulation to examine the paths, and evaluation of the candidate path based on the dynamic mobility index. The most feasible path in this study has been determined as a path which requires the least energy consumption. This is reasonable since the energy consumption can be considered as a gross cost of the rover stability, wheel slippage, and elapsed time required.

The demonstration for the proposed strategy has also been described. Four typical candidate paths have been generated by varying weighting factors for the path planning algorithm. The dynamic simulations of 4-wheeled rover have provided the dynamic mobility indices for each candidate path. The demonstration has confirmed that the most feasible path can be found through the quantitative evaluation based on the dynamic mobility index.

Also, in practical scenario, uncertainties of the soil parameters used for the dynamic simulation should be considered. Incorporating the proposed strategy in this paper with the robotic mobility analysis under uncertain terrain reported in[14] would be useful for more robust/feasible path planning and evaluations.

References

1) A. Stentz, "Optimal and efficient path planning for partially-known environments," in *Proc. of the 1994 IEEE Int. Conf. on Robotics and Automation*, San Diego, CA, pp. 3310-3317.

2) J. Barraquand, B. Langlois, and J. C. Latombe, "Numerical potential field techniques for robot path planning," *IEEE Trans. on Systems, Man and Cybernetics*, vol. 22, no. 2, pp. 224-241, 1992.

3) L. E. Kavraki, P. Svestka, J.-C. Latombe, and M. H. Overmars, "Probabilistic roadmaps for path planning in high-dimensional configuration spaces," *IEEE Trans. on Robotics and Automation*, vol. 12, no. 4, pp. 566-580, 1996.

4) P. Cheng, Z. Shen, and S. M. LaValle, "RRT-based trajectory design for autonomous automobiles and spacecraft," *Archives of Control Sciences*, vol. 11, no. 3-4, pp. 167-194, 2001.

5) B. Donald, P. Xavier, J. Canny, and J. Reif, "Kinodynamic motion planning," *Journal of the ACM*, vol. 40, no. 5, pp. 1048-1066, 1993.

6) C. Urmson, and R. Simmons., "Approaches for heuristically biasing RRT growth," in *Proc. of the 2003 IEEE/RSJ Int. Conf. on Intelligent Robots and Systems*, Las Vegas, NV, pp. 1178-1183.

7) Y. Kuwata, J. Teo, S. Karaman, G. Fiore, E. Frazzoli, and J. How, "Real-time Motion Planning with Applications to Autonomous Urban Driving," *IEEE Trans. on Control Systems Technology*, vol. 17, no. 5, pp. 1105-1118, 2009.

8) T. Howard and A. Kelly, "Trajectory and Spline Generation for All-Wheel Steering Mobile Robots," in *Proc. of the 2006 IEEE Int. Conf. on Intelligent Robots and Systems*, Beijing, China, pp. 4827-4832.

9) K. Iagnemma and S. Dubowsky, *Mobile Robots in Rough Terrain: Estimation, Motion Planning, and Control with Application to Planetary Rovers*, Springer Tracts in Advanced Robotics, 2004.

10) A. Howard, H. Seraji, and E. Tunstel, "A Rule-Based Fuzzy Traversability Index for Mobile Robot Navigation," in *Proc. of the 2001 IEEE Conf. on Robotics and Automation*, Seoul, Korea, pp. 3067-3071.

11) S. Singh, R. Simmons, T. Smith, A. Stentz, V. Verma, A. Yahja, and K. Schwehr, "Recent Progress in Local and Global Traversability for Planetary Rovers,", in *Proc. of the 2000 IEEE Conf. on Robotics and Automation*, San Francisco, CA, pp. 1194-1200.

12) A. Gibbesch and B. Schäfer, "Multibody system modelling and simulation of planetary rover mobility on soft terrain," in *Proc. of 8th Int. Symp.on Artificial Intelligence, Robotics and Automation in Space, i-SAIRAS*, Munich, Germany, 2005.

13) G. Ishigami, A. Miwa, K. Nagatani, and K. Yoshida, "Terramechanics-Based Model for Steering Maneuver of Planetary Exploration Rovers on Loose Soil," *Journal of Field Robotics*, vol. 24, no. 3, pp. 233-250, 2007.

14) G. Ishigami, G. Kewlani, and K. Iagnemma, "Predictable Mobility," *IEEE Robotics and Automation Magazine*, vol. 16, no. 4, pp. 61-70, 2009.

15) D. Helmick, A. Angelova, L. Matthies, C. Brooks, I. Halatci, S. Dubowsky, and K. Iagnemma, "Experimental Results from a Terrain Adaptive Navigation System for Planetary Rovers," in *Proc. of 9th Int. Symp. on Artificial Intelligence, Robotics and Automation in Space, i-SAIRAS*, Hollywood, CA, 2008.

16) Steven M. LaValle; *PLANNING ALGORITHMS*, Cambridge University Press, 2006.

17) J. Wong, *Theory of Ground Vehicles*. 4th Ed., New York, Wiley, 2008.

18) G. Ishigami, K. Nagatani, and K. Yoshida, "Slope Traversal Controls for Planetary Exploration Rover on Sandy Terrain," *Journal of Field Robotics*, vol. 26, no. 3, pp. 264-286, 2009.

19) Y. Yokokoji, S. Chaen, and T. Yoshikawa, "Evaluation of Traversability of Wheeled Mobile Robots on Uneven Terrains by Fractal Terrain Model," in *Proc. of the 2004 IEEE Int. Conf. on Robotics And Automation*, Sendai, Japan, pp. 2183-2188.

20) H. Nakashima, Y. Shioji, K. Tateyama, S. Aoki, H. Kanamori, and T. Yokoyama, "Specific Cutting Resistance of Lunar Regolith. Simulant under Low Gravity Conditions," *Journal of Space Engineering*, vol. 1, no. 1, pp. 58-68, 2008.